ISSN: 2639-7455

Research Article

Earth & Environmental Science Research & Reviews

A Planet Crossing the Fragment Chain of a Large Comet

Hamid A. Rafizadeh[1*] and Rama Bhargavi Vempolu[2]

[1]*Emeritus Professor, Bluffton University, USA*

[2]*Graduate student, Computer Science Department, University of Dayton, USA.*

[*]Corresponding Author
Hamid A. Rafizadeh, Emeritus Professor, Bluffton University; Adjunct Professor, University of Dayton. Present Address: 320 Northview Road, Oakwood, OH 45419, USA.

Submitted: 2024 Mar 12; **Accepted**: 2024 May 15; **Published**: 2024 May 24

Citation: Rafizadeh, H. A., Vempolu, R. B. (2024). A Planet Crossing the Fragment Chain of a Large Comet. *Earth Envi Scie Res & Rev, 7*(2), 01-16.

Abstract

Using two models, the Graphical Sequence Model (GSM) and the Orbital Configuration Model (OCM), this study investigates the interaction between a planet and a large comet's fragment chain. The GSM, applied through Python coding, predicts a planet's average number of fragment crossings and the probability of capture. Using OCM we find that upon crossing, a significant fraction of fragments escape, a notable percentage gets captured and forms a near-spherical shell around the planet, and a smaller number impacts the planet. Applying GSM to the fragment chain of a 100-km-diameter comet's fully fragmented chain, the planet crosses an average of about 32 thousand fragments with an average capture probability of 5.33×10^{-2} *per crossing per perihelion passage. OCM results indicate that 58.8% of crossed fragments escape, 36.7% are captured in orbit around the planet, and 4.5% impact the planet. The distinctive feature of OCM calculations lies in the near-spherical planetary shell formed by captured fragments. The planetary shell dynamics is analyzed in relation to the planet's Roche limit. The capture simulation with fluid fragments moving at the planet speed demonstrates that 4.2% are fully within, 23.7% are partially within, and 72.1% are outside the Roche limit.*

Keywords: Comets, Comets, Dynamics, Impact Processes, Planetary Dynamics

1. Introduction

A recent article, focused on small comets, yielded insights on planets crossing a comet's fragment chain. Motivated by these findings, our attention now shifts to large comets. The earlier study introduced the Graphical Sequence Model (GSM), a general multi-generational model of a comet's fragment chain, to study the probabilities associated with a planet crossing a small comet's fragment chain. Applying GSM to a 3.14-km-diameter comet we found the average probability for a planet crossing the fragment chain of a long period comet as 0.43×10^{-3} per perihelion passage, and for a short period comet, 1.01×10^{-3} per perihelion passage. Regardless of the comet's period, the average probability of fragment capture in chain crossing was 5.84×10^{-2} per crossing. This analysis concluded that the probability for a planet crossing a fragment chain and capturing fragments in chain crossing is higher than the planet-comet collision probability of the order of 10^{-9} per perihelion passage, making chain crossing and fragment capture more probable planetary events [1].

In complexity, large comet GSM calculation differ from small comets as GSM creates a multi-generational structure of comet's fragment chain, with each generation differing in clustering of fragment clumps. The complexity arises from the number of fundamental fragments comprising the comet and its clumps. A 100-km-diameter comet contains 2.6 million fundamental fragments, contrasting with the 81 fundamental fragments in a 3.14-km-diameter comet. In the study of the 3.14-km-diameter comet, GSM fragment chain construction was graphically executed, followed by simulated probability calculations. For the 100-km-diameter comet's fragment chain, the graphical approach becomes unwieldy, especially in later generations. To overcome this computational challenge, GSMPython, a Python tool, is developed to facilitate GSM construction of fragment chains for any generation and comet size. This code is particularly valuable for generating and studying fragment chains of large comets, especially at later stages in fragment chain's lifecycle [1].

In Section 2, GSMPython constructs the multi-generational fragment chains for the 100-km-diameter comet, emphasizing generations 4 and 20 for comparing typical fragment distributions and the probability of fragment capture at chain crossing. Section 3 introduces the Orbital Configuration Model (OCM), applying it to calculate probabilities of fragment capture, escape, and impact. Section 3 calculations highlight a distinctive feature, the formation of a near-spherical planetary shell by captured fragments. Section 4 assesses the spherical shell of captured fragments in relation to fragments impacting the planet. The focus of Section 4 is on outlining the scope for future studies of fragment impact in relation to the near-spherical planetary shell formed by captured fragments. Section 5 provides concluding observations.

2. A Planet Crossing A Large Comet's Fragment Chain

The Graphical Sequence Model (GSM) represents the multi-generational structure of a comet's fragment chain through parameters n_f, n_s, and d_s as shown in Fig. 1 [1]. In each GSM generation, n_f sets the modular fragmentation, while ns and ds establish the pattern of fragment separation. The GSM design assumes a comet comprises a clump of fundamental units, which, in each generation's fragmentation, breaks down into nf smaller clumps that then separate at ns separation units, each of the length ds. This sequence persists until generation nmax, beyond which, only fragment separation is considered, as all units are already fragmented to their fundamental level.

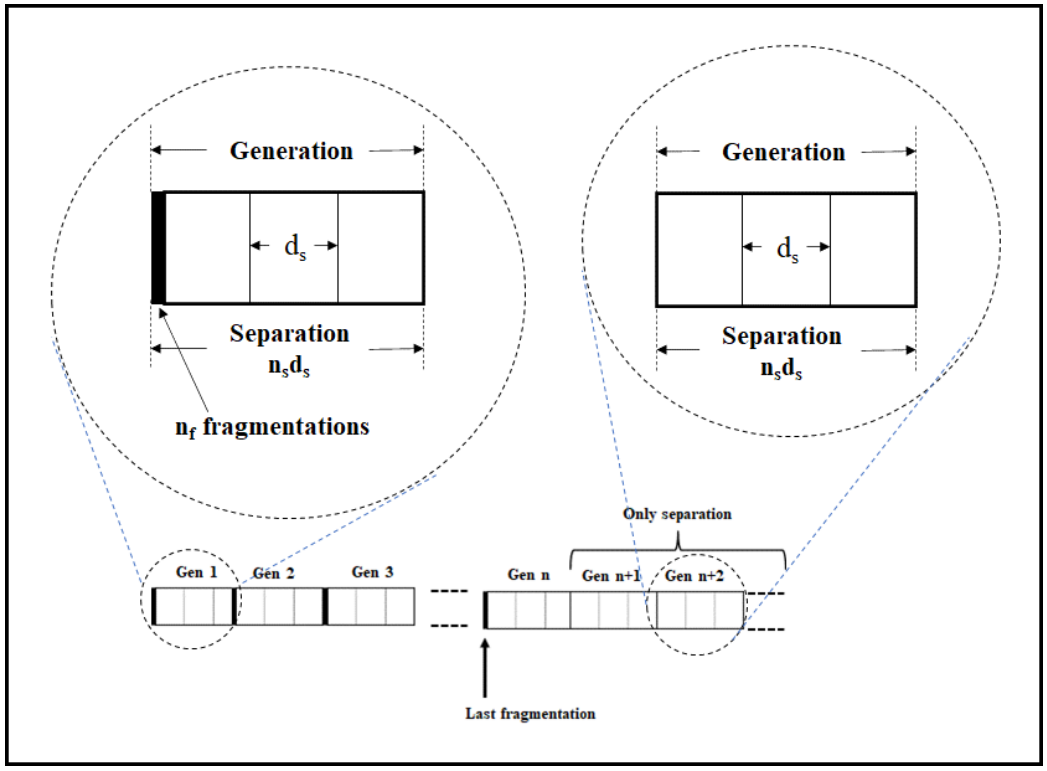

Figure 1. The Graphical Sequence Model (GSM) features a multi-generational modular structure where each generation undergoes fragmentation into n_f clumps, followed by separation of clumps by n_s separation units, each of the length d_s. Fragmentation stops when the comet breaks into fundamental units, after which each new generation only deals with fragment separation.

As representative of large comets, we have chosen a 100-km-diameter comet with base parameters set to $n_f = 3$ and $n_s = 2$ [1]. Using GSM Python to calculate 20 generations, Fig. 2 shows the fragment distribution in the fragment chains. Fragmentation terminates at generation 14, with succeeding generations created only through fragment separation. Fig. 2 depicts the expansion of the fragment chain's length and reduction in peak during the processes of fragmentation and fragment separation. Each generation presents a different spatial distribution of fragments for planet crossing it.

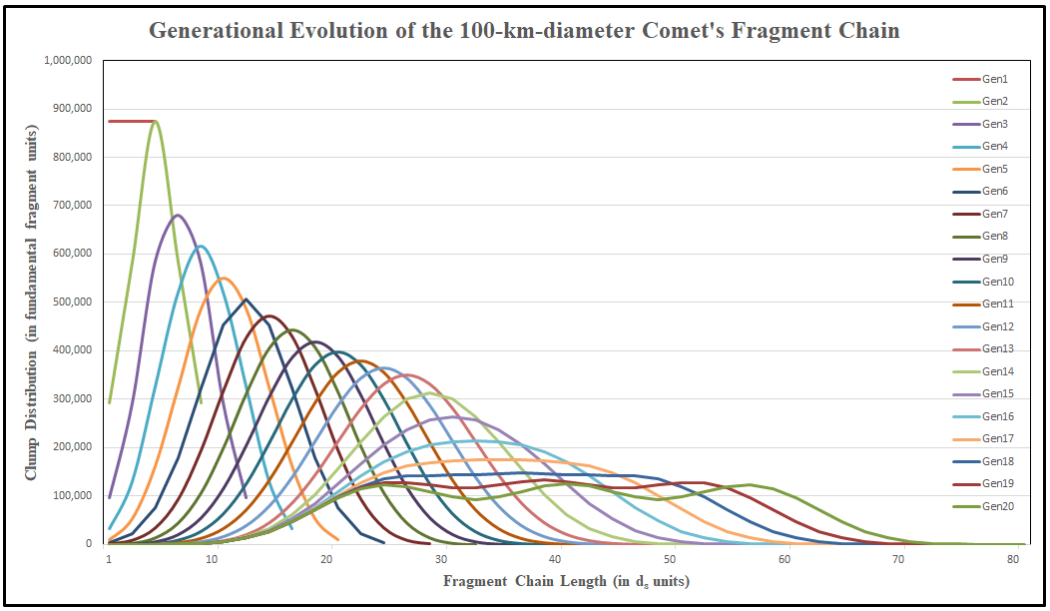

Figure 2: The continuous line charts depict the multi-generational fragment distributions of a 100-km-diameter comet with n_f = 3 and n_s = 2, intentionally excluding gaps in the fragment chain for improved comparative clarity.

In Fig. 3 GSM is extended to 100 generations, revealing the overall pattern of key statistical parameters for the 100-km-diameter comet's fragment chains. From generation 25, the fragment chains' peak reaches an equilibrium value at about 120,000 fragments, while the average number of fragments drops to about 13,000 by generation 20, and continues to decline with each subsequent generation, reflecting the lengthening of the fragment chain.

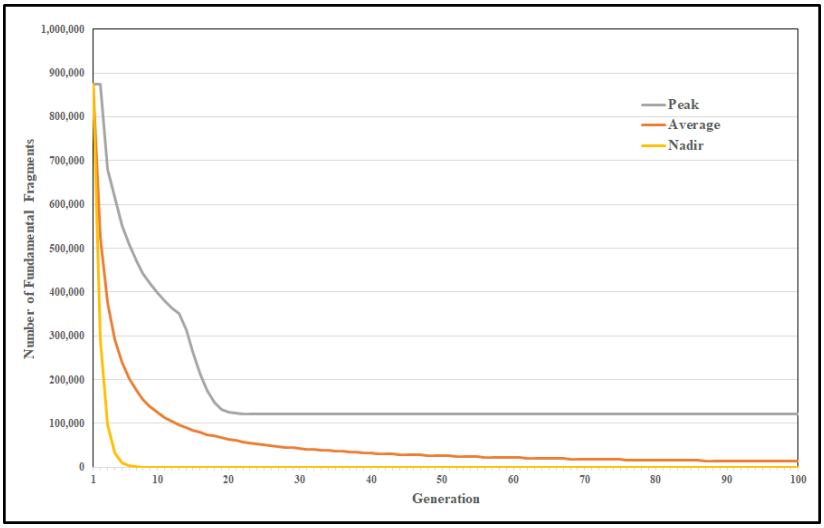

Figure 3. The comparison of 100 generations of fragment chains of a 100-km-diameter comet with n_f = 3 and n_s = 2.

2.1. Fragments Crossed and Probability of Capture

In the GSM framework outlined in Fig. 1, two distinct domains stand out: one where both fragmentation and separation occur, and another where only separation is present. To exemplify this, in the 100-km-diameter comet with n_f = 3 and n_s = 2, we chose generation 4 to showcase fragmentation and separation, and generation 20 for separation only. Their graphical juxtaposition and comparison is presented in Fig. 4.

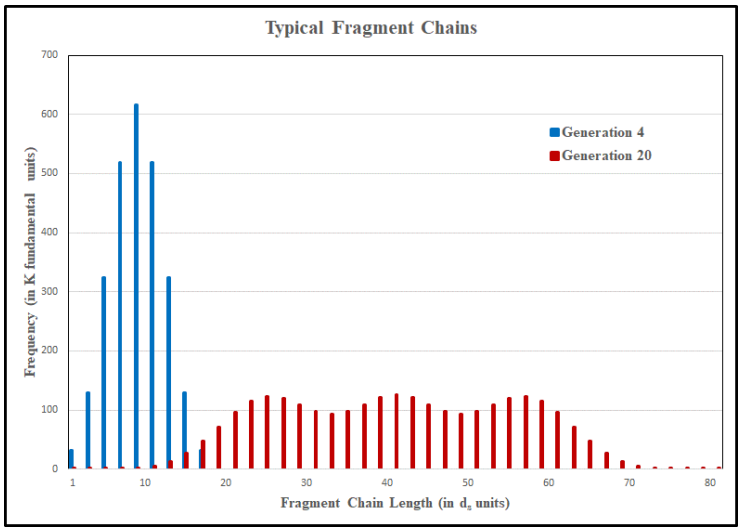

Figure 4. The typical fragment distributions in the fragment chains of the 100-km-diameter comet with $n_f = 3$ and $n_s = 2$.

In these calculations, GSM assumes a 5,000 km diameter for the fragment chain, and a 5-degree intercept angle for the orbits of the planet and the fragment chain. The XYZ positions of crossed fragments are randomly distributed within the space between the radius of the fragment chain and d_s, and the planet is assumed to have an Earth-like velocity of 30 km/s. Relative planet-fragment velocities are randomly generated from a distribution of fragment velocities within the 20 to 40 km/s range.

Using a simulation program, Fig. 5 compares GSM calculations for fragments crossed by the planet in fragment chains of generations 4 and 20 of a 100-km-diameter comet [2]. Generation 4 represents a chain of large clumps, while generation 20's chain is made only of fundamental fragments. The analytical results of these two examples are representative of the entire spectrum of fragment chains depicted in Fig. 2.

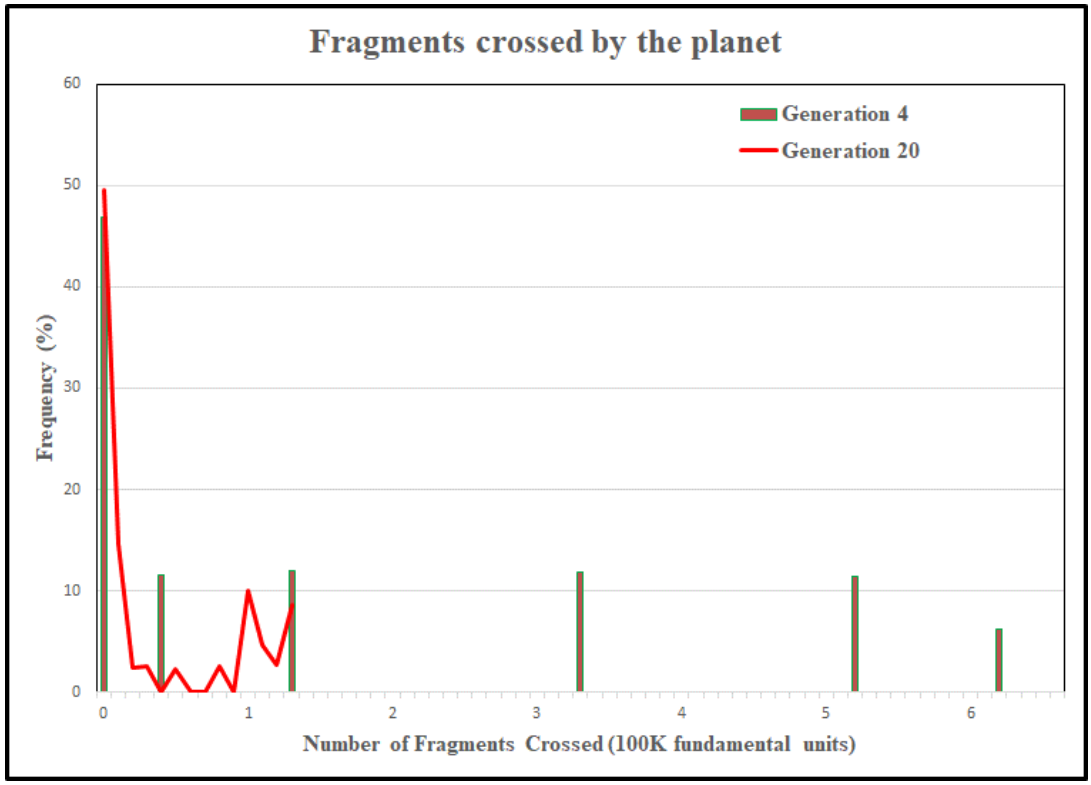

Figure 5. The distribution of the number fragments crossed by the planet in fragment chains of two typical generations of the 100-km-diameter comet with $n_f = 3$ and $n_s = 2$.

The key observation in Fig. 5 is the sheer number of fragments a planet can encounter during a single crossing. Crossing the fragment chain of a large comet may result in encounters with hundreds of thousands of fragments. As such, the situation is not an encounter of a single fragment with the planet, but the planet interacting with a considerably large number of fragments. In our simulations of the 100-km-diameter comet, the average number of fragments crossed is about 155 thousand in generation 4, and about 32 thousand in generation 20.

How long does the planet take to cross a comet's fragment chain? Assuming a fragment chain cylinder with diameter d and intercept angle θ, the planet's path through the chain would have the length $l_p = d / \sin\theta$. The crossing time, t_c, is calculated as $t_c = l_p / |\bar{V}_p - \bar{V}_{fc}|$, where $\bar{V}_p$ is the planet's orbital velocity, $\bar{V}_{fc}$ the fragment chain's velocity at the point of crossing, and $|\bar{V}p - \bar{V}fc|$ the relative speed. For an order-of-magnitude estimate, considering an Earth-like planetary orbital speed of 30 km/s, and a planet-fragment chain relative speed of 10 km/s, Table 1 displays the time for the planet to cross a comet's fragment chain. The crossing time is approximately of the order of a few hours.

Chain-crossing time (hours)		Fragment Chain Diameter (10^3 km)		
		5	**10**	**15**
Intercept angle (°)	**5**	1.59	3.19	4.78
	10	0.80	1.60	2.40
	15	0.54	1.07	1.61

Table 1. The time the planet takes to cross a comet's fragment chain as a function of the diameter of the fragment chain's cylinder and the angle of intercept θ.

Having developed a picture of the fragments encountered when the planet crosses a large come's fragment chain, in the next section we address the probability of fragment capture during such crossings.

2.2. Probability of the Comet Capturing Fragments

In changing a fragment's orbit from chain-centric to planet-centric, the probability of fragment capture during chain crossing depends on eccentricity e and the semi-minor axis b where the capture conditions include eccentricity $e < 1$ and the semi-minor axis $b > R$, with R the planet's radius. These criteria ensure the captured fragment is in orbit around the planet rather than on a trajectory to impact the planet or escape. Given these parameters and defining capture as the transformation of a fragment's chain-centric orbit into a planet-centric orbit, the probability of fragment capture at chain crossing, denoted by $P_{capture}$, can be expressed as:

$$P_{capture} = N(e<1, b>R) / N_{cross.} \quad (1)$$

Here, N_{cross} represents the total number of fragments crossed and $N(e<1, b>R)$ refers to fragments with eccentricity e less than one, indicating elliptical orbits. b represents the semi-minor axis of the fragment's orbit, $R_{\square}$ is the planet's radius, and the condition $b > R$ ensures that the captured fragment is in orbit around the planet, as opposed to impacting it. In the following section on OCM calculations we will address the fragment impact in detail. The eccentricity e in Eq. (1) is determined from equations [3]:

$$\bar{\boldsymbol{e}} = [(V^2 - \mu/r)\,\bar{\boldsymbol{r}} - (\bar{\boldsymbol{r}} \bullet \bar{\boldsymbol{V}})\,\bar{\boldsymbol{V}}]/\mu, \text{ and} \quad (2)$$

$$e = |\,\bar{\boldsymbol{e}}\,|. \quad (3)$$

$\bar{\boldsymbol{V}}$ represents the planet-fragment relative velocity, $\bar{V}_p - \bar{V}_{fc}$, where $\bar{V}_p$ is the planet velocity and $\bar{V}_{fc}$ the fragment chain velocity. $\bar{\boldsymbol{r}}$ is the XYZ position of the fragment, and the gravitational parameter μ, for an Earth-like planet, is taken as 3.986×10^5 km3 s^{-2}. Assuming the planet's orbit intersects the fragment chain's orbit at angle θ, $\bar{V}_p$ is positioned at an angle θ relative to $\bar{V}_{fc}$. The purpose of these calculations is to obtain the orbital relationships between a comet fragment and the planet. This methodology assumes that in fragment-planet interaction, the planet is the dominant gravitational force (sun and other planets negligible because of the relative distances). Assuming two-body motion, the corresponding orbital elements can be calculated using the position and velocity of the fragment and planet. The fragment's orbital elements are calculated with the semimajor axis an indicator of whether the orbit is elliptical around the planet or hyperbolic and parabolic where the fragment escapes.

Factors favoring fragment capture include a small intercept angle θ, a small relative velocity in planet-fragment chain interaction, and both the planet and the fragment chain moving in counterclockwise orbits. In such a configuration, the relative velocity plays a crucial role in fragment capture, with a smaller relative velocity increasing the probability of fragment capture [4]. As such, in the initial simulation of fragment capture in chain

crossing, the intercept angle θ is set at 5 degrees.

In the calculation of Eq. (1), the semi-minor axis b is determined from the eccentricity and semi-major axis a [3]:

$$b = a\sqrt{(1-e^2)} \quad (4)$$

where semi-major axis a is

$$a = -\tfrac{1}{2}\,\mu / (V^2/2 - \mu/r). \quad (5)$$

In Fig. 6, simulation calculations compare the number of fragments captured per crossing in generations 4 and 20 of a 100-km-diameter comet. Generation 4 exhibits a higher number of fragments captured than generation 20, on average about 294,000 fundamental fragments in generation 4, and 67,000 in generation 20. The maximum numbers captured are 616,000 fundamental fragments in generation 4 and 126,000 in generation 20. Despite these differences, the probabilities of fragment capture for the two generations are similar. On average, the simulated probability of fragment capture when the planet crosses the generation 4 fragment chain is 5.44×10^{-2} per crossing, compared to generation 20's average fragment capture probability of 5.33×10^{-2} per crossing.

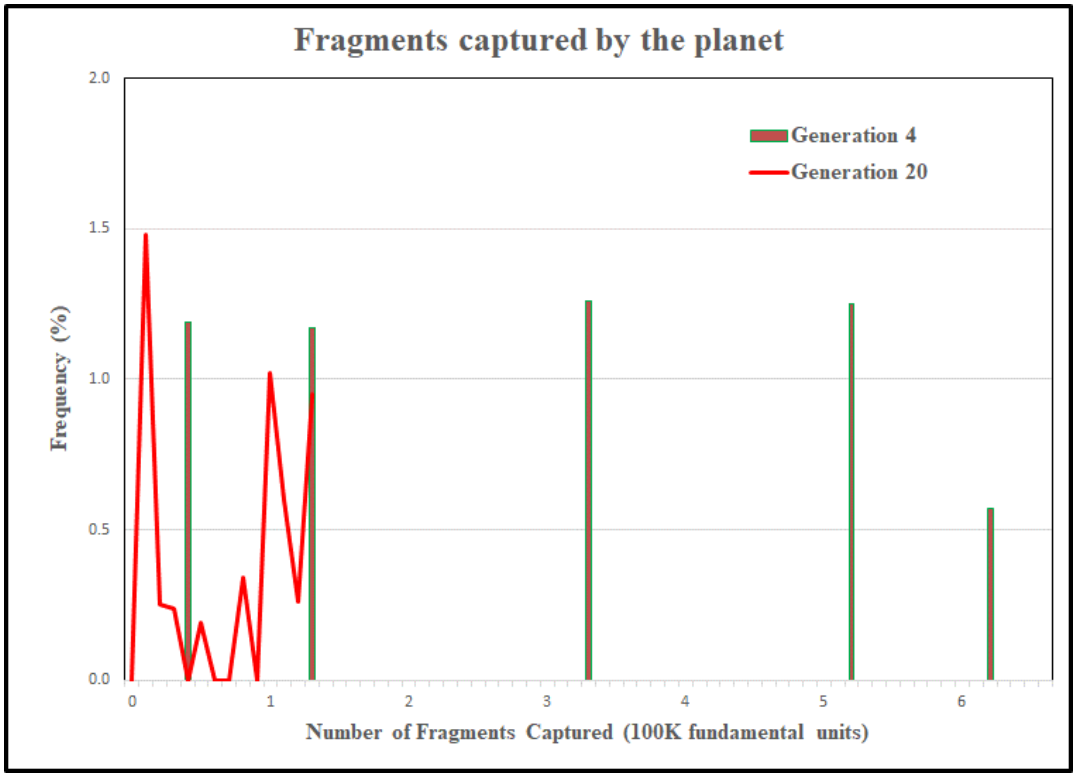

Figure 6. The distribution of the fragments captured when the planet crosses the fragment chain of a 100-km-diameter comet with $n_f = 3$ and $n_s = 2$.

Having applied GSM to analyze fragments crossed and the probability of fragment capture, the next section explores normalized OCM calculations for the probabilities of fragment capture, fragment escape, and fragment impact when a planet crosses a fragment chain.

3. Orbital Configuration in Chain Crossing

In this section, the Orbital Configuration Model (OCM) is introduced and applied to calculate probabilities of fragment capture, fragment escape, and fragment impact, complementing GSM calculations. OCM, illustrated in Fig. 7, is derived from the orbital configuration when a planet crosses a fragment chain and presents an astrophysical perspective of the planet and comet revolving counterclockwise around the Sun with a small intercept angle. It establishes the structural elements specific to the planet crossing the fragment chain's cylinder, and provides the details of the parameters used in OCM calculations.

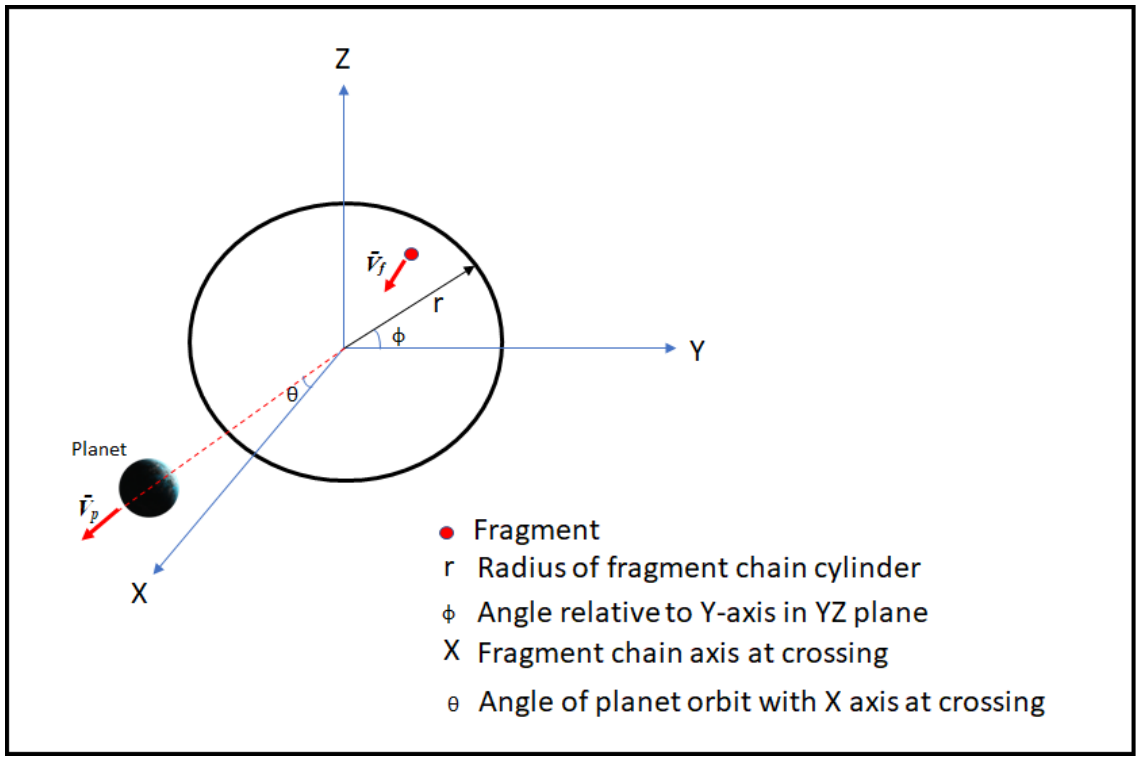

Figure 7. The Orbital Configuration Model (OCM) elements for calculating and analyzing capture, escape, and impact probabilities when a planet crosses a comet's fragment chain.

At the chain crossing point, the fragment chain's cylinder is assumed to move along the X axis with the speed $\bar{V}_{fc} = (V_x, 0, 0)$. In simulation calculations, the planet velocity $\bar{V}_p$ is considered Earth-like at 30 km/s, with components derived from $V_x = V_p \cos\theta$, $V_y = V_p \sin\theta \cos\phi$, and $V_z = V_p \sin\theta \sin\phi$, where θ is the angle between the orbits of the planet and the fragment chain at the crossing point, and ϕ is the angle relative to Y axis in the YZ plane.

For the fragment chain velocity at the crossing point, a range of 20 to 40 km/s is supported by Minor Planet Center (MPC) database of the known comets [1]. In this article's simulation calculations, V_{fc} is varied between 25 and 35 km/s, enveloping the assumed planet speed of 30 km/s. This introduces low relative velocities that amplify fragment capture possibilities. The study specifically focuses on small θ values because in modeling a planet crossing a comet's fragment chain, the dissipative mechanism contributing to fragment capture comes largely from the small relative velocities of the planet and the fragment chain, requiring a small intercept angle. In simulation calculations, the intercept angle is assumed to take values of 5, 10, and 15 degrees.

In OCM calculations, the planet is assumed to be Earth-like with a diameter of 13,000 km. Along the X axis, the domain for random planet-fragment encounters spans 1 to 20 planet radii on both sides of the planet as it traverses the fragment chain. The X coordinate of the fragment is randomly selected within this space. A fragment's radial position rf is assumed to be randomly situated in increments of 10% of the fragment chain's cylinder diameter r. The angle ϕ is varied randomly in 10-degree increments from zero to 360 degrees. The Y and Z coordinates of the fragments are calculated as $Y = r_f \cos\phi$ and $Z = r_f \sin\phi$.

In OCM calculations, random variations of XYZ, V_p, V_{fc}, θ, and ϕ have been normalized to 10,000 fragments encountered by the planet. This normalization ensures comparability across all parametric scenarios without the need to normalize calculations to per fragments encountered. Additionally, this normalization renders the calculations independent of the comet size or the distribution of fragments in a generation's fragment chain.

In OCM simulation calculations, the first parameter considered is the normalized distribution of eccentricity e. Using Eqs. (2–3), the eccentricity calculations determine the number of fragments that escape an encounter with the planet ($e < 1$) and those that are either captured around the planet or impact the planet ($e < 1$). Fig. 8 shows the simulated normalized distribution of fragments interacting with the planet, revealing that 41.2% of the encountered fragments have eccentricity less than 1 and are either captured in orbit around the planet or impact the planet.

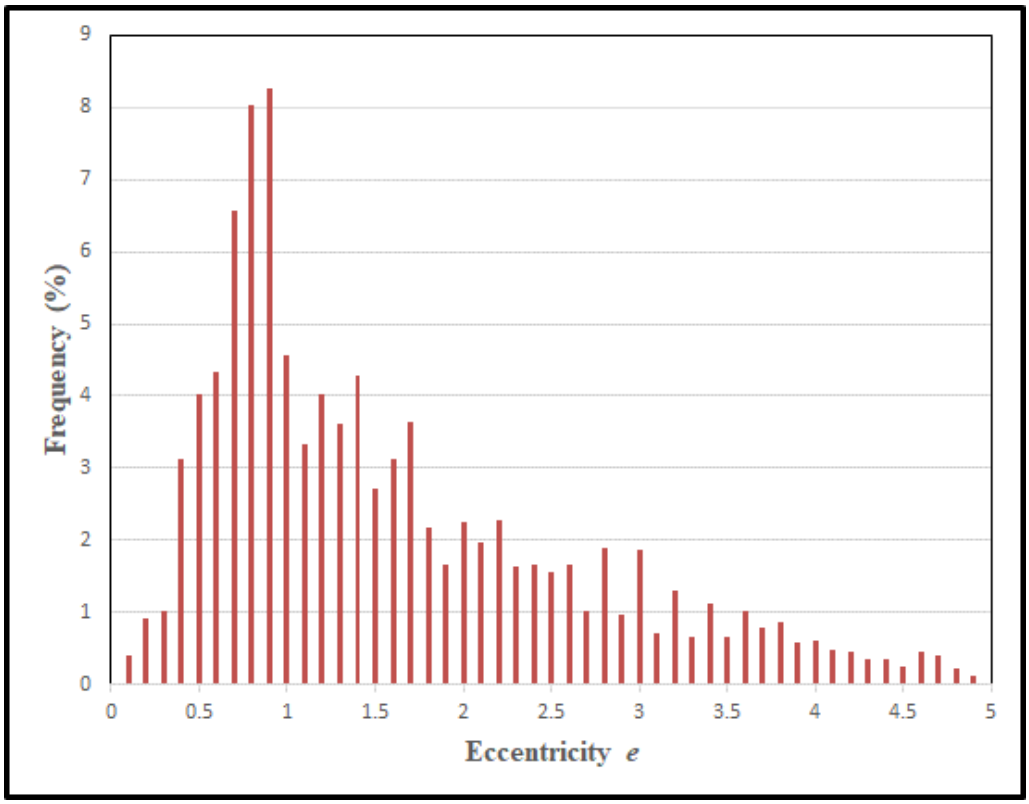

Figure 8. Normalized eccentricity distribution of fragments either captured around the planet or impacting the planet (e < 1) or escaping (e ≥ 1).

The eccentricity calculations alone do not differentiate the percentage of fragments captured or impacting the planet. This information is obtained from the simulated calculation of the fragments' semi-minor axis. As impact condition, it is assumed that any orbit with a semi-minor axis less than the planet radius would correspond to an impacting fragment. This assumption does not consider the planet atmosphere. In the normalized OCM calculation of *b*, using Eqs. (4–5), 4118 fragments have eccentricities less than one, out of which 447 fragments have a semi-minor axis less than 6500 km, signifying impact. In the normalized simulation of chain crossing, this corresponds to 4.5% of the fragments impacting the planet, 36.7% captured in orbit around the planet, and 58.8% of fragments escaping.

The normalized simulation of the distribution of the semi-major axis a reveals an interesting feature in Fig. 9, which displays a values in the range of 0 to 130,000 km for fragments captured around the planet. The inset shows the entire simulated *a* range, indicating 10.5% of the fragments have a semi-major axis greater than 130,000 km, and 58.8% have negative semi-major axes. This leaves 30.7% of the fragments with semi-major axis values between 0 and 130,000 km, enabling a comparison with the planet's Roche limit, *d*.

Given an Earth-like planet, the Roche limit *d* is about 18,000 km for a rigid fragment and about 34,000 km for a fluid fragment [5]. Among fragments captured within the range of zero to 130,000 km, 54% lie within the fluid Roche limit of 34,000 km, and 31% fall within the rigid Roche limit of 18,000 km. It is assumed that fragments within the Roche limit, whether fluid or rigid, will break apart upon capture in orbit around the planet.

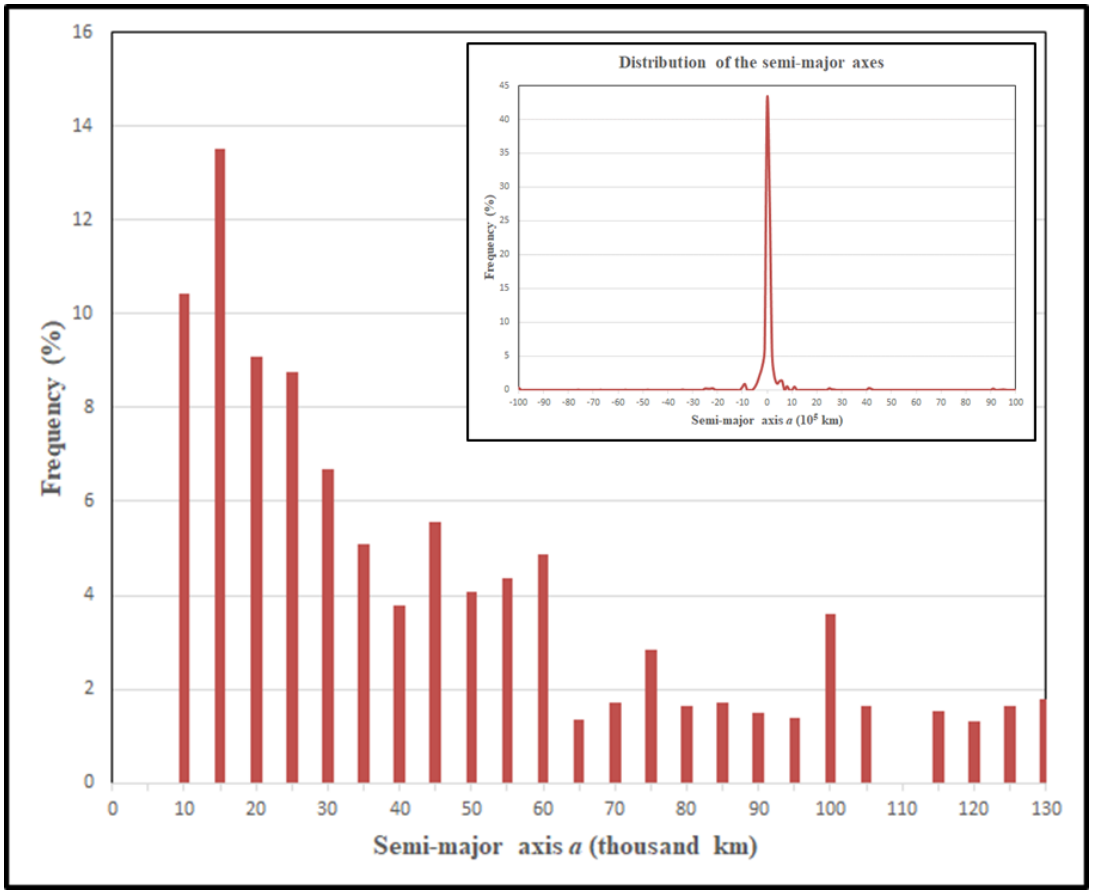

Figure 9. Distribution of the semi-major axis *a* of the fragments captured around the planet.

When compared to the Roche limit radius d, the semi-major axis a only identifies the fragments that are fully captured within the Roche limit ($a < d$), resulting in the immediate breakup of these fragments and the formation of a shell of cometary dust and debris around the planet. In contrast, the semi-minor axis b provides information on fragments whose orbits only partially pass through the Roche limit ($a > d$, but $b < d$). The breakup for these fragments occurs more gradually compared to those fully captured within the Roche limit (a < d).

Fig. 10 shows the simulated distribution of captured fragments that are partially within the Roche limit ($a > d$, and $b < d$). For visual clarity of the horizontal axis for smaller b values, the chart does not include 1,393 of the 2,137 fragments with b values greater than 70,000 km that always lie outside the Roche limit.

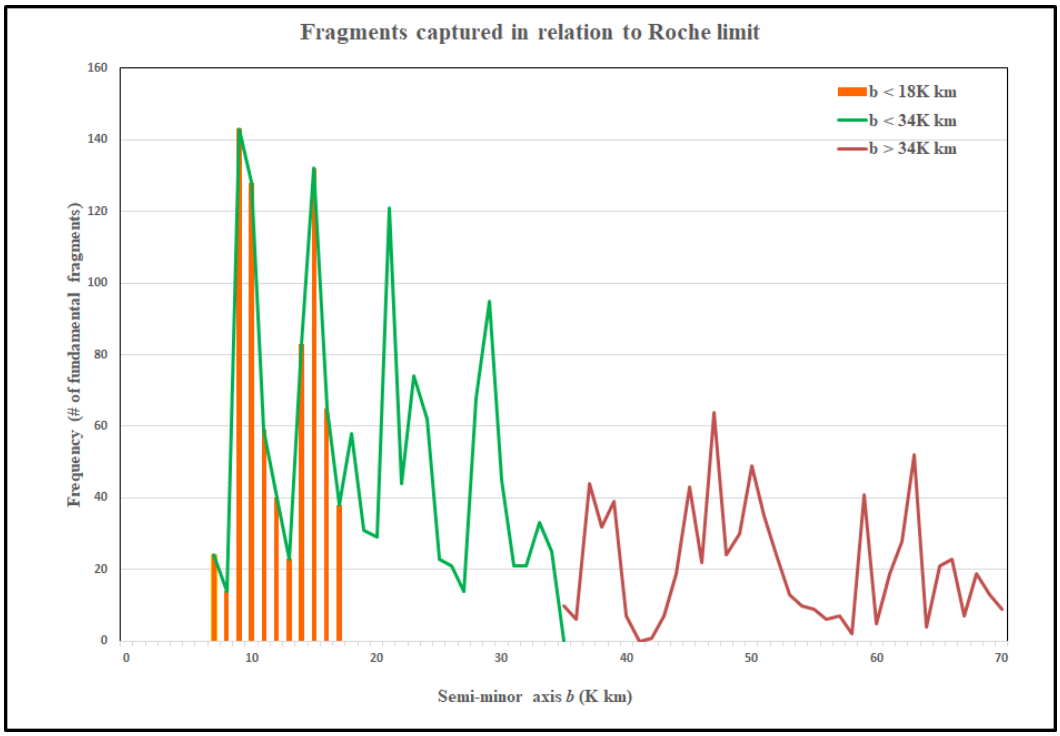

Figure 10. The simulated distribution of fragments with semi-minor axis b within the Roche limit and semi-major axis a outside the Roche limit ($a > d$, $b < d$). These fragments experience slower breakdown compared to fragments fully captured within the Roche limit ($a < d$).

3.1. Structure of Captured Fragments

The semi-major axis a depicts the structural framework for distribution of captured fragment in relation to the Roche limit and the semi-minor axis *b* delineates the impacting fragments and characterizes the fragments fully or partially passing within the Roche limit. An additional source of information comes from the inclination of fragments captured around the planet. The inclination *i* is given as [3]:

$$i = \mathrm{Cos}^{-1}(h_z/|\bar{\boldsymbol{h}}|), \text{ where } \bar{\boldsymbol{h}} = \bar{\boldsymbol{r}} \times \bar{\boldsymbol{V}}.$$

OCM inclination calculations (see Fig. 11) suggest captured fragments form an almost spherical pattern around the planet, organized in two distinct layers. The inner layer, within the planet's Roche limit, consists of dust and debris from broken fragments. The outer layer is primarily composed of fragments as originally captured. Fragments partially breaching the Roche limit temporarily reside in the second layer, contributing to the first layer's dust and debris. The detailed dynamics of this planetary shell will be explored in future studies.

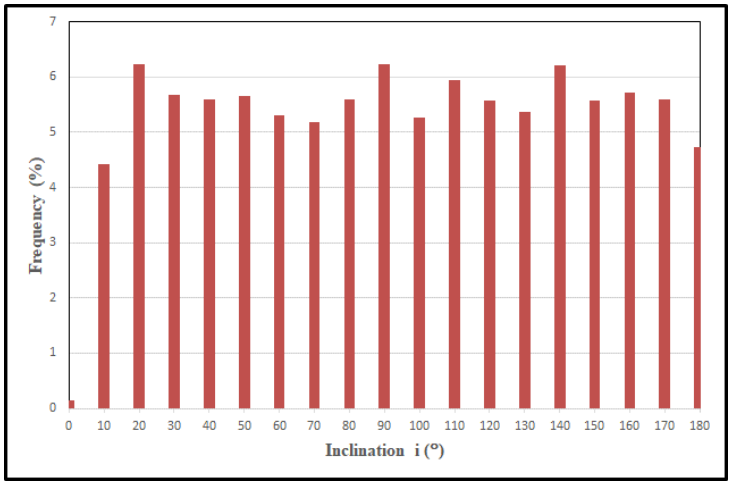

Figure 11. The normalized distribution of the inclination i of fragments captured in orbit around the planet.

The inclination calculation for impacting fragments also shows a roughly near-spherical structure in their orbits, indicating a corresponding near-spherical distribution of impact points on the planet's surface. The geometric basis for the distribution of captured fragments in the planetary shell, and the fragments impacting the planet remains the same. Both the captured and impacting fragments originate from a near-spherical planetary shell. For an Earth-like planet, this configuration suggests that about 71% of impacts will occur in oceans.

3.2. OCM Parametric Views

In OCM calculations, parameters XYZ, V_p, V_{fc}, θ, and ϕ were initially varied randomly to simulate the planet-fragment chain interactions. This section focuses on highlighting a specific parameter for comparative evaluations. For example, Table 2 maintains constant intersect angle while simulating specific fragment velocities. The calculations indicate that as the fragment velocity approaches the planet's velocity—as relative velocity decreases, the result, as expected, is a higher number of captured fragments. At a fragment speed of 30 km/s, where the fragment and planet are moving at the same speed, 82.2% of encountered fragments are either captured in orbit or impact the planet. At fragment speeds of 25 km/s and 35 km/s, the simulated fragment capture and number of fragments impacting the planet remain similar.

Fragment velocity V_x (km/s)	**20**	**25**	**30**	**35**	**40**
Total fragments crossed by planet	10,000	10,000	10,000	10,000	10,000
Total fragments escaped	10,000	8,771	1,777	8,778	10,000
Total fragments captured or impacting	0	1,229	8,223	1,222	0
% of total escaped	100.0%	87.7%	17.8%	87.8%	100.0%
% of total captured or impacting	0.0%	12.3%	82.2%	12.2%	0.0%
Total captured in orbit around the planet	0	825	7,708	907	0
Total fragments impacting planet (b < 6,500 km)	0	404	515	315	0
% captured impacting planet	NA	32.9%	6.3%	25.8%	NA
% captured and orbiting the planet	NA	67.1%	93.7%	74.2%	NA

Table 2. The normalized simulation of the planet crossing the comet's fragment chain, showing fragments captured or impacting (e < 1) and fragments escaping (e ≥ 1) as a function of the fragment velocity V_x with the intersect angle fixed at θ = 5°.

Fig. 12 shows the normalized inclination distribution of all captured fragments as a function of fragment velocity V_x. This distribution is almost uniform at all inclinations and retains a near-spherical configuration irrespective of variations in fragment speed. The normalized inclination distribution of the impacting fragments as a function of fragment velocity V_x is similar to the captured fragments. However, the distribution is quasi-spherical, as variations at all inclinations cannot be described as uniform, indicating that the captured fragments exhibit a higher degree of spherical geometry compared to fragments impacting the planet. The inclination distribution of impacting fragments as a function of the intercept angle θ shows a similar pattern. Smaller intercept angles exhibit a uniform, near-spherical planetary pattern, while larger intercept angles result in a less uniform, and less spherical distribution.

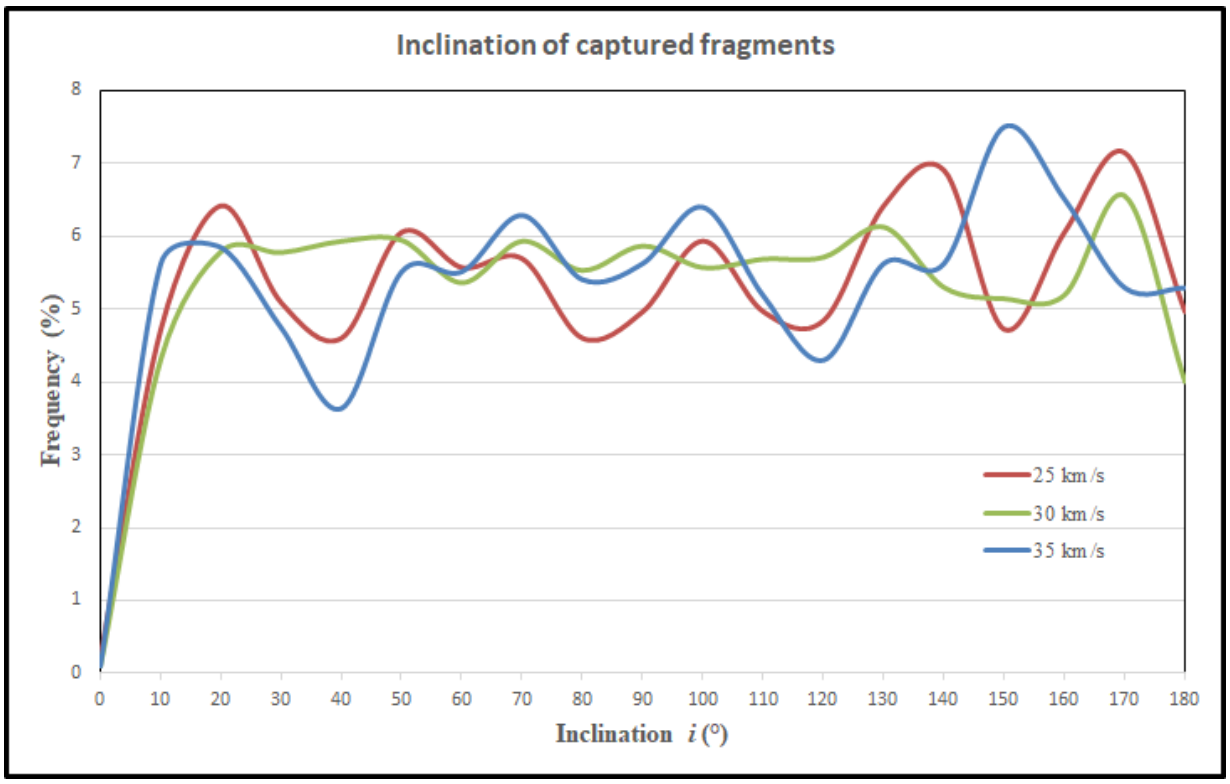

Figure 12. The normalized distribution of the inclination *i* of captured fragments as a function of fragment velocity V_x.

Focusing on the Roche limit, the fragments captured completely within the Roche limit are assumed to disintegrate promptly, while those that lie outside may break apart gradually or accrete into larger fragments. Tables 3 and 4 show the simulated normalized distribution of fragments with Earth-like rigid Roche limit (18,000 km) and fluid Roche limit (34,000 km). Fragments fully within the Roche limit ($a < d$) break up, forming a planetary shell of cometary dust and debris. Fragments with orbits partially pass through the Roche limit ($a > d$, $b < d$) break up more slowly. For all V_x values and rigid fragments, the count of those fully within the Roche limit is consistently lower than those partially within it. The closer the fragment speed to the planet speed, the portion of fragments outside of the Roche limit increases. At a fragment speed of 30 km/s, assuming rigid fragments, only 1.9% are fully within, 13.5% are partially within, and 84.6% are totally outside the Roche limit. With fluid fragments, 4.2% are fully within, 23.7% are partially within, and 72.1% are outside the Roche limit.

Fragment velocity V_x (km/s)	**20**	**25**	**30**	**35**	**40**
Total fragments crossed	10,000	10,000	10,000	10,000	10,000
Total fragments captured	0	1,229	8,223	1,222	0
Fragments impacting the planet, $b < 6500$ km	0	404	515	315	0
Fragments passing through the rigid Roche Limit, $b < d$	0	544	1266	512	0
Fragments fully within rigid Roche limit, $a < d$	0	89	154	139	0

Fragments partially passing through the rigid Roche limit, $a > d$, $b < d$	0	455	1112	373	0
% of partially in the Roche limit in relation to total captured	NA	37.0%	13.5%	30.5%	NA
% of fully in the Roche limit in relation to total captured	NA	7.2%	1.9%	11.4%	NA

Table 3. Simulation of the rigid fragments fully or partially captured inside the Roche limit as a function of fragment velocity. The intersect angle is 5°.

Fragment velocity V_x (km/s)	**20**	**25**	**30**	**35**	**40**
Total fragments crossed	10,000	10,000	10,000	10,000	10,000
Total fragments captured	0	1,229	8,223	1,222	0
Fragments impacting the planet, $b < 6500$ km	0	404	515	315	0
Fragments passing through the fluid Roche Limit, $b < d$	0	815	2294	667	0
Fragments fully within fluid Roche limit, $a < d$	0	353	344	389	0
Fragments partially passing through the fluid Roche limit, $a > d$, $b < d$	0	462	1950	278	0
% of partially in the Roche limit in relation to total captured	NA	37.6%	23.7%	22.7%	NA
% of fully in the Roche limit in relation to total captured	NA	28.7%	4.2%	31.8%	NA

Table 4. Simulation of the fluid fragments fully or partially captured inside the Roche limit as a function of fragment velocity. The intersect angle is 5°.

In the preceding OCM calculations of this section, we maintained a constant intercept angle at 5 degrees. Varying the intercept angle θ in increments of 1, 5, 10 and 15 degrees to simulation of the rigid or fluid fragments fully or partially captured inside the Roche limit as a function of the intersect angle θ produces results similar to Tables 3 and 4. A smaller intercept angle results in a higher number of fragments captured in orbit around the planet. At the same time, at small angles, the number of fragments impacting the planet is also high. Conversely, a large intercept angle leads to fewer captured fragments within the planet's Roche limit.

4. Shell formation and Impact Dynamics

As pointed out in previous OCM analysis, the planet's interaction with a comet's fragment chain extends beyond capture and escape, involving fragment impacts on the planet, culminating in potentially catastrophic events. Captured fragment with a semi-minor axis smaller than the planet's radius are considered impacting fragments. In this assumption OCM does not consider

the planet's atmosphere.

OCM calculations challenge the conventional impact paradigm, which envisions an apocalyptic outcome with a singular strike causing prolonged solar radiation shutdowns and impact winters [6,7]. The dire perspective intensifies exponentially when hundreds of fragments, rather than a single fragment, strike the planet. This view suggests widespread extinction due to the combined intensity of numerous impacts and the extended solar shutdown during the ensuing impact winter. However, OCM, as a model of a chain-crossing planet, reframes this narrative.

Unlike a singular impact's dispersion of dust and debris in planet's upper atmosphere, the chain-crossing perspective characterizes impact as "local" due to the planetary shell formed by captured fragments. The falling cometary debris from the planetary shell dampens the upward flow of the impact plumes, providing a different outcome.

Setting up the concept of the Plume Repression Factor (PRF) to measure the relationship between captured and impacting fragments, and defining the number of fragments within or partially passing through the Roche limit as N_{wp} and the number of fragments impacting the planet as N_{impact}, the Plume Repression Factor (PRF) can be characterized as:

$$PRF = N_{wp} / N_{impact}$$

Table 5 contrasts the fragment content of the planetary shell for potential downward flow with the number of impacting fragments, using the Plume Repression Factor (PRF). The calculation of PRF, assuming either rigid or fluid fragments, highlights the observation that the downward flow of materials from captured fragments can not only exist over much longer time periods compared to up-to-a-few-hours duration of impacts, but in volume, it can be multiples of the size of fragments impacting the planet. We note that PRF, as a rough measure, does not consider the upward-thrown planet material as impact products. More detailed models are needed for a comprehensive understanding of multiple impacts within a planetary shell of cometary dust and debris.

Fragment velocity V_x (km/s)	**20**	**25**	**30**	**35**	**40**
Fragments impacting the planet, $b < 6500$ km	0	404	515	315	0
Fragments passing through rigid Roche Limit, $b < d$	0	544	1266	512	0
Fragments passing through fluid Roche Limit, $b < d$	0	815	2294	667	0
Rigid fragment Plume Repression Factor	NA	1.35	2.46	1.63	NA
Fluid fragment Plume Repression Factor	NA	2.02	4.45	2.12	NA

Table 5. Simulation of the ratio of the fragments captured within the Roche limit countering fragments impacting the planet, varying with fragment velocity V_x at a fixed intersect angle of 5°.

4.1 Younger Dryas impact hypothesis

The Younger Dryas impact hypothesis posits a causative connection between a cosmic impact event and the onset of the Younger Dryas (YD) climate cooling episode at about12,800 calendar years before present (BP). Substantiating evidence includes a peak in continental-scale biomass burning, the extinction of a large genera of North American Pleistocene megafauna, and the disappearance of the Paleoindian Clovis culture [7,8]. The idea of fragments from a large disintegrating comet impacting earth, and depositing peak concentrations of platinum, high-temperature spherules, meltglass, and nanodiamonds, spans a global footprint that includes more than 50 sites across four continents, affecting both the Northern and Southern Hemispheres [9]. The suggested source is a 100-km-diameter comet that arrived about 20,000 to 30,000 years ago from the centaur system in an earth-crossing orbit and disintegrated to form today's Taurid Complex [10,11].

Applying Di Sisto et al.'s model for comet fragmentation and chain formation [12], Napier extends beyond a singular impact, proposing the hypothesis that the Younger Dryas (YD) impact is the result of earth's encounter with the fragment chain of a 100-km-dameter comet in an Encke-like orbit [13].

The current studies on Younger Dryas impact hypothesis predominantly adopt an impact-centric perspective, whether considering a fragment or a fragment swarm, and they face the difficulty of explaining a global phenomenon within the impact's short time period. The chain-crossing model of a planet developed in this article adds a novel explanation that sees the global presence of the YD event not a result of an impact event but rather the outcome of a "shell collapse." As the shell formed in chain crossing becomes unstable and eventually collapses, the result would be equivalent to global impacts and airbursts that

would radically change the planet's climate conditions, adversely affecting its megafauna and inhabitants. The "shell collapse" presents a more comprehensive and plausible explanation for the global manifestations of the Younger Dryas event.

4.2 Future studies

Our study of a planet crossing a comet's fragment chain reveals that the material falling planetward from the planetary shell within the Roche limit counteracts the plumes of dust and debris resulting from fragment impacts. The slowly falling wave of cometary material, predominantly water, mitigates the upward-moving plume, confining the damage locally rather than allowing global dispersion in the planet's upper atmosphere. The dynamics of these counterflowing material streams, localizing the impact damage, presents an important area for future planetary science studies in modeling interactions between a planet and a comet's fragment chain.

In future studies, it becomes imperative to address the dynamics of the planetary shell. Cho and Polvani demonstrated that a planetary shell, modeled as a "thin, homogeneous layer of fluid with a free surface, moving under the influence of gravitational and Coriolis forces," organizes into banded structures with a polar vortex [14]. Investigating whether a comparable phenomenon manifests in the planetary shell of cometary matter, and determining if the banding and polar vortex facilitate sunlight reaching the planet, giving the banded shell a quasi-equilibrium state before its collapse, are crucial aspects of planetary shell formation through chain crossing. These aspects warrant in-depth and detailed studies in future research endeavors.

Another research direction involves fragments impacting oceans, leading to immediate consequences such as tsunamis. How would tsunamis, generated from multiple impact sites, all occurring within a short timeframe, interact? From Table 1, at a 5-degree intercept angle, with a fragment chain diameter of 5,000 km, the planet's chain-crossing time would be 1.59 hours. The impacts into the oceans and the subsequent tsunami formation, occurring within a span of a few hours, necessitate a comprehensive study of the details and dynamics of randomly generated tsunamis. This research is crucial for understanding the complexities inherent in the planet crossing a comet's fragment chain, particularly in contrast to the formation of a single tsunami from a solitary impact.

5. Concluding Observations

By applying the Graphical Sequence Model (GSM) to study multi-generational fragment chains from a large 100-km-diameter comet, we observe that the planet, in crossing the chain, undergoes a staggering number of interactions with fragments. The development and application of the Orbital Configuration Model (OCM) to a planet crossing a comet's normalized fragment chain, reveal two key observations. First, captured fragments form near-spherical distributions around the planet. Second, the dynamic balance between the captured and impacting fragments prevents, or at least minimize, the adverse effects of plumes of dust and debris thrown into the upper atmosphere by fragment impacts.

A significant contribution of this article lies in shedding light on future planetary science studies, particularly regarding the capture of a large number of fragments around the planet, forming a planetary shell, and the concurrent impacts by an large number of fragments when the planet crosses a large comet's fragment chain.

Acknowledgements

We would like to thank Professor Kerry D. Hicks of AFIT for support in development of OCM.

Notes

1 The Python code for GSM calculations is available at https://drive.google.com/drive/folders/1C_QF7_Bpjp2ZVEnXOKt-jkLFkSGkcrl_g?usp=drive_link. The details of the code, including algorithms are available here. The output for the fragment chains of selected generations can be downloaded as a CSV file.

Statements and Declarations

Declaration of Competing Interests: The authors have no conflicts of interest to disclose.

Funding: This research did not receive any specific grant from funding agencies in the public, commercial, or not-for-profit sectors.

References

1. Rafizadeh, H.A., 2024. Analyzing a planet that crosses a small comet's fragment chain. *Earth & Environmental Science Res. & Rev. 7*(2), 1–14.
2. Nester, D., 2019. Excel Simulation Package. Bluffton University.
3. Hicks, K. D. (2009). *Introduction to astrodynamic reentry* (pp. 18-19). Air Force Institute of Technology.
4. Wetherill, G. W., & Stewart, G. R. (1993). Formation of planetary embryos: Effects of fragmentation, low relative velocity, and independent variation of eccentricity and inclination. *Icarus, 106*(1), 190-209.
5. Roche limit. 2023. In Space Wiki. https://space.fandom.com/wiki/Roche_limit.
6. Lyons, S. L., Karp, A. T., Bralower, T. J., Grice, K., Schaefer, B., Gulick, S. P., ... & Freeman, K. H. (2020). Organic matter from the Chicxulub crater exacerbated the K–Pg impact winter. *Proceedings of the National Academy of Sciences, 117*(41), 25327-25334.
7. Wolbach, W. S., Ballard, J. P., Mayewski, P. A., Adedeji, V., Bunch, T. E., Firestone, R. B., ... & Kennett, J. P. (2018). Extraordinary biomass-burning episode and impact winter triggered by the Younger Dryas cosmic impact 12,800 years ago. 1. Ice cores and glaciers. *The Journal of Geology, 126*(2), 165-184.
8. Moore, C. R., West, A., LeCompte, M. A., Brooks, M. J., Daniel Jr, I. R., Goodyear, A. C., ... & Bunch, T. E. (2017). Widespread platinum anomaly documented at the Younger Dryas onset in North American sedimentary sequences. *Scientific reports, 7*(1), 44031.

9. Pino, M., Abarzúa, A. M., Astorga, G., Martel-Cea, A., Cossio-Montecinos, N., Navarro, R. X., ... & Kennett, J. P. (2019). Sedimentary record from Patagonia, southern Chile supports cosmic-impact triggering of biomass burning, climate change, and megafaunal extinctions at 12.8 ka. *Scientific reports, 9*(1), 4413.
10. Clube, S. V. M., & Napier, W. M. (1984). The microstructure of terrestrial catastrophism. *Monthly Notices of the Royal Astronomical Society, 211*(4), 953-968.
11. Steel, D. I., & Asher, D. J. (1996). The orbital dispersion of the macroscopic Taurid objects. *Monthly Notices of the Royal Astronomical Society, 280*(3), 806-822.
12. Di Sisto, R. P., Fernández, J. A., & Brunini, A. (2009). On the population, physical decay and orbital distribution of Jupiter family comets: Numerical simulations. *Icarus, 203*(1), 140-154.
13. Napier, W. M. (2019). The hazard from fragmenting comets. *Monthly Notices of the Royal Astronomical Society, 488*(2), 1822-1827.
14. Cho, J. Y. K., & Polvani, L. M. (1996). The emergence of jets and vortices in freely evolving, shallow-water turbulence on a sphere. *Physics of Fluids, 8*(6), 1531-1552.